IEEE Access
Multidisciplinary | Rapid Review | Open Access Journal

Received February 14, 2019, accepted February 25, 2019, date of publication March 11, 2019, date of current version March 29, 2019.

Digital Object Identifier 10.1109/ACCESS.2019.2904228

Using the Stator Current Ripple Model for Real-Time Estimation of Full Parameters of a Permanent Magnet Synchronous Motor

KYUNGHWAN CHOI[1], YONGHUN KIM[1], KYUNG-SOO KIM[1], (Member, IEEE), AND SEOK-KYOON KIM[2]

[1]Department of Mechanical Engineering, Korea Advanced Institute of Science and Technology, Daejeon 34141, South Korea
[2]Department of Creative Convergence Engineering, Hanbat National University, Daejeon 341-58, South Korea

Corresponding authors: Kyung-Soo Kim (kyungsookim@kaist.ac.kr) and Seok-Kyoon Kim (lotus45kr@gmail.com)

This work was supported by the grant (Development of Hybrid Electric Vehicle Conversion Kit for Diesel Delivery Trucks and its Commercialization for Parcel Services) from the Transportation and Logistics Research Program (TLRP) funded by the Ministry of Land, Infrastructure and Transport of the Korean Government under Grant 17TLRP-C135446-01.

ABSTRACT In this paper, a new method is proposed for the real-time estimation of the full parameters of a permanent magnet synchronous motor (PMSM) that is based on the stator current ripple model. By introducing the stator current ripple model together with the known two state equations for the d- and q-axes currents, we resolve the rank deficiency problem, thus enabling real-time full parameter estimation even in the steady state. A signal processing technique for removing adverse effects from noises and uncertainties existing in the stator current ripple measurement is also presented. The efficacy of the proposed method is verified by simulation on a 15-kW PMSM, and both the proposed and conventional methods are compared.

INDEX TERMS Permanent magnet synchronous motor (PMSM), rank deficiency, real-time parameter estimation, stator current ripple.

I. INTRODUCTION

Accurate knowledge of the electrical parameters of a permanent magnet synchronous motor (PMSM) (i.e., d- and q-axes inductances, stator resistance, and flux linkage) is required for high-performance PMSM drive systems.

In terms of the efficiency of the PMSM, parameter information can be used to generate the optimal current references that minimize copper or iron loss in the known control methods. These references are the maximum torque per current (MTPC), flux weakening (FW), and maximum torque per voltage (MTPV) [1]–[4]. Current controllers such as proportional integral (PI) controllers and disturbance compensators [5], [6], which are used to precisely track the generated current references, can also be designed using the parameter information. The accuracy of the parameter information has a considerable impact on the efficiency of the PMSM and the transient performance of the current control.

For the reliability and robustness of the PMSM drive system, the parameter information can be utilized for online stator winding fault diagnosis [7], [8], demagnetization detection of permanent magnets in rotor [9], stator/rotor condition monitoring [10], and position [11] or current [12] sensorless control.

However, accurately identifying those parameters that cannot be directly measured is quite difficult, and they can even vary according to operating conditions. To address this problem, many techniques for accurate estimation of the PMSM parameters have been previously proposed, which are classified into offline identification and online estimation algorithms.

Techniques for offline identification of PMSM parameters are based on finite-element analysis (FEA) of the PMSM [13] or the steady-state d- and q-axes voltage equations obtained from offline measurements under various operating conditions [14]. The identification results are then stored in a processor as look-up tables (LUT). However, offline identification not only requires expensive experimental or simulation efforts to obtain the LUTs, but also additional memory allocation of the processor [13]. More importantly, the LUTs obtained offline cannot deal with changes in the PMSM parameters resulting from

The associate editor coordinating the review of this manuscript and approving it for publication was Auday A.H. Mohamad.

aging, temperature hikes, or abnormal operations such as demagnetization [15].

Online parameter estimation algorithms used to overcome the disadvantages of offline methods have been proposed in many studies. These are based on the recursive least-squares (RLS) method [15], model-reference adaptive system (MRAS) [16], adaptive techniques [17], sliding mode observer (SMO) [18], and extended Kalman filter (EKF) [19]. All of these methods are based on the PMSM d- and q-axes state equations, which only guarantee rank two in the steady state. Therefore, they can estimate (at most) two parameters simultaneously based on the assumption that the other two parameters are known by measurements or nominal values. In other words, the estimation of all four parameters is impossible because of the 'rank deficiency' of the state equations [20]. Any attempt to estimate three or four parameters does not guarantee convergence, because the estimation results fall into a null space generated by the rank deficiency [21].

To enable online full parameter estimation, applying the signal injection to online estimation methods was previously considered to collect more sets of the PMSM state equations and thus increasing the rank [21]–[23]. The signal injection methods applied to a neural network estimator [21] and RLS [22] showed successful results for three- and four-parameter estimations, respectively. However, the amplitude of the injected signal is usually set sufficiently large to ensure a high signal-to-noise ratio, which may introduce considerable disturbance and instability into the PMSM drive system [24] and lead to increased torque ripple or copper loss. In [25], two affine-projection-algorithm (APAs)-based online full parameter estimation techniques were proposed for separately estimating the slow-varying (stator resistance and flux linkage) and fast-varying (d- and q-axes inductances) parameters, in which two parameters are fixed to estimate the others. However, the parameter interdependence for the separate estimation and convergence of the solution was not rigorously handled.

This study proposes a new online full parameter estimation method for PMSM to solve the rank deficiency problem. The purpose of the proposed method is to utilize two additional ranks hidden in the newly introduced stator current ripple model. These ranks help to establish a full-rank estimation model together with the known two state equations. The RLS algorithm for the full-rank estimation model allows for an online full parameter estimation, even in the steady state when not relying on a signal injection or a separate estimation of the slow- and fast-varying parameters. A signal processing technique for removing adverse effects from noises and uncertainties that exist in the stator current ripple measurement is also presented. The simulation results for various operating conditions of a 15-kW PMSM demonstrate the efficacy of the proposed method as compared to that of the conventional signal injection method.

II. STATOR CURRENT RIPPLE MODEL

A. GENERAL DESCRIPTION OF PMSM IN ROTATING D-Q FRAME

In a synchronous rotating d-q frame, the electrical dynamics of the PMSMs [26] can be described by:

$$L_d \frac{di_d}{dt} = -R_s i_d + w_r L_q i_q + v_d, \tag{1}$$

$$L_q \frac{di_q}{dt} = -R_s i_q - w_r (L_d i_d + \phi_m) + v_q, \tag{2}$$

$$T_e = \frac{3p}{4}(\phi_m i_q + (L_d - L_q) i_d i_q), \tag{3}$$

where i_d, i_q, v_d, and v_q denote the d-and q-axes stator currents and input voltages, respectively, and, T_e, w_r, and p are the electrical output torque, electrical rotor speed, and number of poles, respectively. The electrical parameters L_d, L_q, R_s, and ϕ_m represent the d- and q-axes inductances, stator resistance, and flux linkage, respectively.

The four electrical parameters are usually assumed to be constant for controller design, but various factors can affect their values. The stator resistance and flux linkage are highly influenced by variations in motor temperature [9] having slow dynamics, which allows us sufficient time to estimate the two parameters. However, the d- and q-axes inductances are considerably affected by the magnetic saturation of the stator windings [27] that have the same fast dynamics as the d- and q-axes stator currents, which require a fast and robust estimation algorithm.

The input voltages v_d and v_q are generated by switching operation of a voltage source inverter (VSI) with space vector pulse width modulation (SVPWM). The time average of one zero and two active voltage vectors in a switching period forms the effective average voltages of v_d and v_q. A transient-state can be observed in the switching period because of the application of different space voltage vectors, which produces a 'stator current ripple,' even in the steady state where the average voltages of v_d and v_q are constant.

The d- and q-axes state equations used in the conventional parameter estimation techniques are models for the average voltages, but the transient-state within a switching period has not been previously considered. The core of this study is to identify two additional ranks hidden in the stator current ripple dynamics, which is derived in Section II-B. A signal processing technique for removing noises or uncertainties present in the stator current ripple measurements is proposed in Section II-C.

B. DERIVATION OF THE STATOR CURRENT RIPPLE MODEL

An example of the d- and q-axes stator current measurements as a function of the voltage vector angle in the α-β frame (θ_V) is given in Fig. 1. The d- and q-axes stator currents contain the following frequency components: the fundamental frequency, three times the voltage vector angular frequency, and harmonics of the switching frequency. The d- and q-axes current envelopes $i_{d,env}$ and $i_{q,env}$, excluding the harmonic

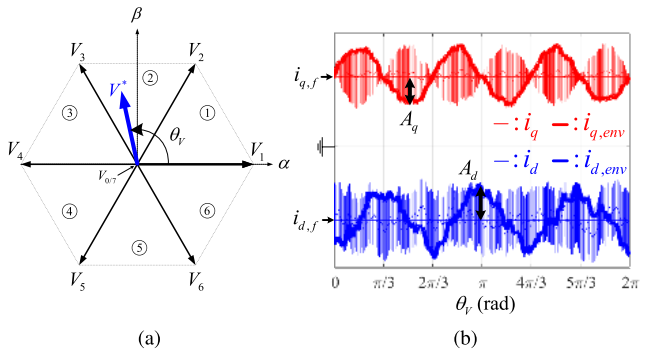

FIGURE 1. Stator current measurements of a PMSM versus voltage vector angle in the α-β frame. (a) Voltage vector in the α-β axis. (b) Stator current measurements in the d-q frame.

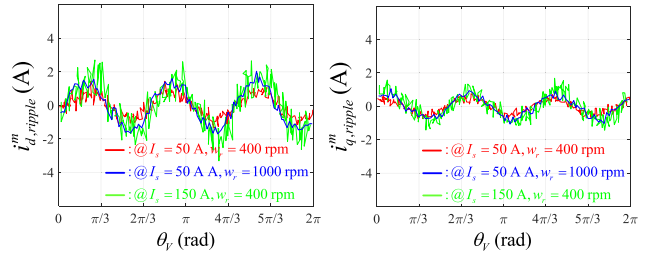

FIGURE 2. Stator current ripple measurement results of a PMSM under three different operating conditions. (a) d-axis current ripple measurements. (b) q-axis current ripple measurements.

components of the switching frequency, can be described by:

$$i_{d,env} = i_{d,f} - A_d \cos(3\theta_V - \varphi_d), \tag{4}$$
$$i_{q,env} = i_{q,f} + A_q \sin(3\theta_V - \varphi_q), \tag{5}$$

where $i_{d,f}$ and $i_{q,f}$ are the fundamental components of the stator currents, A_d and A_q are the amplitudes of the d- and q- axes current ripple components of three times the voltage vector angular frequency, and φ_d and φ_q are the phase delays of the d- and q- axes current ripple components, respectively. The d- and q- axes current ripples $i_{d,ripple}$ and $i_{q,ripple}$ are defined by:

$$\begin{aligned} i_{d,ripple} &= i_{d,env} - i_{d,f} \\ &= -A_d \cos(3\theta_V - \varphi_d), \end{aligned} \tag{6}$$
$$\begin{aligned} i_{q,ripple} &= i_{q,env} - i_{q,f} \\ &= A_q \sin(3\theta_V - \varphi_q). \end{aligned} \tag{7}$$

The switching patterns of SVPWM have a periodicity established through six switching sectors for every one cycle of the voltage vector angle, as shown in Fig. 1, causing the stator current ripple envelopes sinusoidal waveforms to be three times the voltage vector angle. The stator current ripple amplitudes $A_{d(q)}$ and the phase delays $\varphi_{d(q)}$ can vary with operating conditions such as stator current magnitude and rotor speed, which influence the switching pattern of SVPWM for the current control. The measurement results of

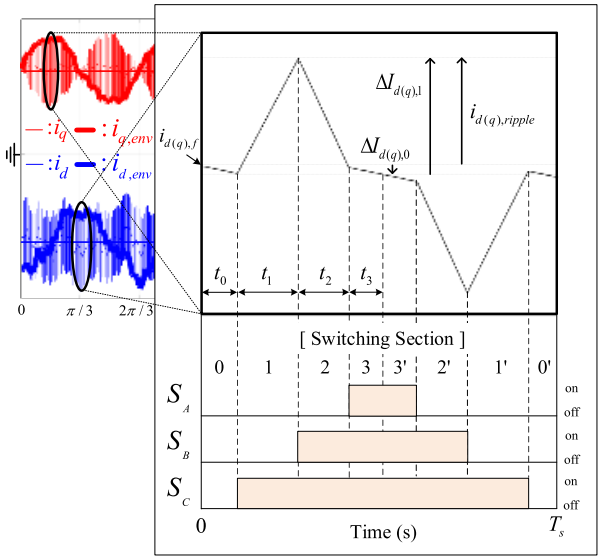

FIGURE 3. Stator current ripple generated by the switching pattern of a VSI with SVPWM.

stator current ripples of a PMSM (which will be used in the simulation study) under three different operating conditions are given in Fig. 2.

The mechanism of the stator current ripple generation based on the switching pattern of a VSI with SVPWM is depicted in Fig. 3, where S_A, S_B and S_C denote the upper switches of phases A, B, and C in a VSI, respectively. There are four switching sections (0, 1, 2, and 3) within one switching period of T_s, and generally the largest current variation occurs at the end of switching section 1, which constitutes the stator current ripple envelopes. The d- and q- axes current ripples $i_{d,ripple}$ and $i_{q,ripple}$ can be modeled by

$$i_{d(q),ripple} = \Delta I_{d(q),0} + \Delta I_{d(q),1}, \tag{8}$$

where $\Delta I_{d(q),0}$ and $\Delta I_{d(q),1}$ are the $d(q)$-axis current variations in the switching sections 0 and 1, respectively:

$$\begin{aligned} \Delta I_{d,i} &= t_i \dot{i}_{d,i} \\ &= \frac{t_i}{L_d}(-R_s i_{d,f} + w_r L_q i_{q,f} + v_{d,i}), \end{aligned} \tag{9}$$
$$\begin{aligned} \Delta I_{q,i} &= t_i \dot{i}_{q,i} \\ &= \frac{t_i}{L_q}(-R_s i_{q,f} - w_r(L_d i_{d,f} + \phi_m) + v_{q,i}), \end{aligned} \tag{10}$$

where t_i, $i_{d(q),i}$, and $v_{d(q),i}$ are the switching interval, $d(q)$-axis current, and input voltage at the switching section i, respectively. By substituting the current variations of (9) and (10) into (8), we can obtain the stator current ripple model as follows:

$$\begin{aligned} i_{d,ripple} &= \left(v_{d,eff} + w_r L_q i_{q,f} - R_s i_{d,f}\right) \frac{t_{eff}}{L_d}, \\ i_{q,ripple} &= \left(v_{q,eff} - w_r \left(L_d i_{d,f} + \phi_m\right) - R_s i_{q,f}\right) \frac{t_{eff}}{L_q}, \end{aligned} \tag{11}$$

where $v_{d(q),eff} = \frac{v_{d(q),0} t_0 + v_{d(q),1} t_1}{t_0 + t_1}$ and $t_{eff} = t_0 + t_1$, which can be calculated from the switching pattern information, the mathematical expressions for which are given in [28].

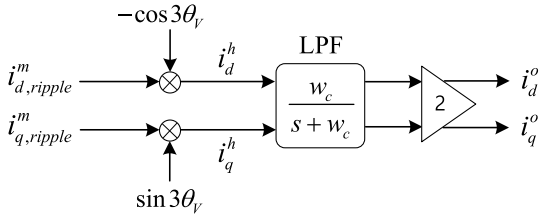

FIGURE 4. Signal processing technique for removing noises or uncertainties present in the stator current ripple measurements.

C. SIGNAL PROCESSING TECHNIQUE FOR CURRENT RIPPLE MEASUREMENT

The measurements of stator current ripples can be obtained based on the differences between the d- and q-axes currents measured at the end of switching section 1 and the start of switching section 0, as described in Fig. 3. However, the stator current ripple values obtained by the measurements themselves contain not only the pure ripple components of (6) and (7) but also zero-mean white noises from current sensors or uncertainties of DC or harmonic components. This is because of the inverter nonlinearity [29] given as follows:

$$i^m_{d(q),ripple} = i_{d(q),ripple} + w + a_0 + \sum_{n=1} a_n \sin(n\theta_V + \varphi_n), \tag{12}$$

where $i^m_{d(q),ripple}$ is the $d(q)$-axis current ripple measurement, w is white noise, and the remaining terms represent uncertainties of DC and harmonic components. If the measurement values are directly applied to the stator current ripple model of (11), the robustness of the model may deteriorate.

The signal processing technique described in Fig. 4 is proposed to attenuate the adverse effects from those noises and uncertainties. First, the stator current ripple measurements $i^m_{d,ripple}$ and $i^m_{q,ripple}$ are multiplied by $-\cos 3\theta_V$ and $\sin 3\theta_V$, respectively, as follows:

$$\begin{aligned} i^h_d &= i^m_{d,ripple}(-\cos 3\theta_V) \\ &= \frac{A_d}{2}\left(\cos\varphi_d + \cos(6\theta_V - \varphi_d)\right) - (w + a_0)\cos 3\theta_V \\ &\quad - \sum_{n=1} \frac{a_n}{2}\left\{\sin\left((n+3)\,\theta_V + \varphi_n\right)\right. \\ &\quad \left. + \sin\left((n-3)\,\theta_V + \varphi_n\right)\right\}, \end{aligned} \tag{13}$$

$$\begin{aligned} i^h_q &= i^m_{q,ripple}\sin 3\theta_V \\ &= \frac{A_q}{2}\left(\cos\varphi_q - \cos(6\theta_V - \varphi_q)\right) + (w + a_0)\sin 3\theta_V \\ &\quad - \sum_{n=1} \frac{a_n}{2}\left\{\cos\left((n+3)\,\theta_V + \varphi_n\right)\right. \\ &\quad \left. - \cos\left((n-3)\,\theta_V + \varphi_n\right)\right\}. \end{aligned} \tag{14}$$

Then, low-pass filters (LPF) applied to i^h_d and i^h_q extract only DC components. The final outputs of the signal processing, which are double the number of extracted DC components, correspond to the following:

$$\begin{aligned} i^o_d &= A_d\cos\varphi_d = i_{d,ripple}\big|_{\theta_V=\frac{1}{3}\pi,\pi,\frac{5}{3}\pi}, \\ i^o_q &= A_q\cos\varphi_q = i_{q,ripple}\big|_{\theta_V=\frac{1}{6}\pi,\frac{5}{6}\pi,\frac{3}{2}\pi}. \end{aligned} \tag{15}$$

The relationships (15) imply that the two outputs of signal processing are the same as the values of $i_{d,ripple}$ at $\theta_V = \frac{1}{3}\pi, \pi, \frac{5}{3}\pi$ and $i_{q,ripple}$ at $\theta_V = \frac{1}{6}\pi, \frac{5}{6}\pi, \frac{3}{2}\pi$, respectively, without any noises or uncertainties except for the third harmonics. Therefore, $i_{d(q),ripple}$ in the stator current ripple model (11) can be replaced by $i^o_{d(q)}$ for the particular voltage vector angle conditions as follows:

$$\begin{aligned} i^o_d &= \left(v_{d,eff} + w_r L_q i_{q,f} - R_s i_{d,f}\right)\cdot\frac{t_{eff}}{L_d}\bigg|_{\theta_V=\frac{1}{3}\pi,\pi,\frac{5}{3}\pi}, \\ i^o_q &= \left(v_{q,eff} - w_r(L_d i_{d,f} + \phi_m) - R_s i_{q,f}\right)\cdot\frac{t_{eff}}{L_q}\bigg|_{\theta_V=\frac{1}{6}\pi,\frac{5}{6}\pi,\frac{3}{2}\pi}, \end{aligned} \tag{16}$$

This makes the stator current ripple model more robust.

To remove the fundamental and harmonic components contained in $i^h_{d(q)}$, the LPF cut-off frequency w_c should be less than half the fundamental frequency (i.e., electrical rotor speed). Simultaneously, the cut-off frequency should be sufficiently high not to interfere with the rapid detection of variations in the stator current ripple amplitudes resulting from PMSM operating condition changes. Accordingly, the cut-off frequency can be set as a function of the electric rotor speed as follows:

$$w_c = \max(K w_r, w_{c,\min}), \tag{17}$$

with $K \le 0.5$ and the minimum value of the cut-off frequency $w_{c,\min}$.

III. ONLINE FULL PARAMETER ESTIMATION SCHEME

By combining the two known d- and q-axes state equations of (1) and (2) with the newly introduced stator current ripple model of (16), a full-rank linear parametric model for the online full parameter estimation can be constructed as follows:

$$y = X\theta, \tag{18}$$

where y, X, and θ are the output vector, the regressor matrix, and the parameter vectors, respectively, which are defined by:

$$\begin{aligned} y &= \begin{bmatrix} v_d & v_q & v_{d,eff} & v_{q,eff} \end{bmatrix}^T, \\ X &= \begin{bmatrix} 0 & -w_r i_{q,f} & i_{d,f} & 0 \\ w_r i_{d,f} & 0 & i_{q,f} & w_r \\ \dfrac{i^o_d}{t_{eff}} & -w_r i_{q,f} & i_{d,f} & 0 \\ w_r i_{d,f} & \dfrac{i^o_q}{t_{eff}} & i_{q,f} & w_r \end{bmatrix}, \\ \theta &= \begin{bmatrix} L_d & L_q & R_s & \phi_m \end{bmatrix}^T. \end{aligned} \tag{19}$$

The RLS algorithm based on the full-rank linear parametric model is used to estimate the all electrical parameters of a

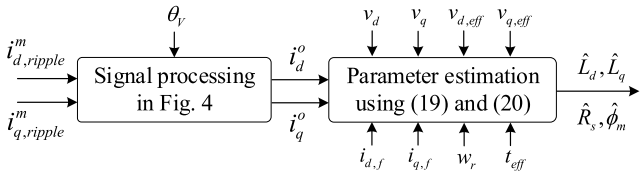

FIGURE 5. Structure of the proposed online full-parameter estimation algorithm.

PMSM as follows:

$$
\begin{aligned}
P_{k+1} &= \frac{1}{\mu}(P_k - P_k X_{k+1}^T(\mu I + X_{k+1}P_k X_{k+1}^T)^{-1}X_{k+1}P_k),\\
\gamma_{k+1} &= P_{k+1}X_{k+1}^T,\\
e_{k+1} &= y_{k+1} - X_{k+1}\hat{\theta}_k,\\
\hat{\theta}_{k+1} &= \hat{\theta}_k + \gamma_{k+1}e_{k+1},
\end{aligned} \tag{20}
$$

where $\hat{\theta} = \left[\hat{L}_d\ \hat{L}_q\ \hat{R}_s\ \hat{\phi}_m\right]^T$ is the estimated parameter vector, e is the estimation error, γ and P are correction gain matrices, μ is the forgetting factor, which is usually selected to be less than 1, and the subscript k represents a calculation step. The third and fourth rows of X_k are updated at $\theta_V = \frac{1}{3}\pi, \pi, \frac{5}{3}\pi$ and $\theta_V = \frac{1}{6}\pi, \frac{5}{6}\pi, \frac{3}{2}\pi$, respectively. The structure of the proposed online full parameter estimation algorithm is depicted in Fig. 5.

Remark: The full rank of the linear parametric model is easily demonstrated by showing that the determinant of X is not zero:

$$
|X| = w_r i_{d,f}\frac{i^o_d i^o_q}{i^2_{eff}} \neq 0. \tag{21}
$$

t_{eff} is always non-zero except in the case when the switching of a VSI operates in six-step mode, whereas i^o_d and i^o_q are always non-zero when the switching is active. Therefore, the non-zero determinant is satisfied under the reasonable condition of $w_r i_{d,f} \neq 0$, which is easily achieved in an interior PMSM (IPMSM), where a non-zero d-axis current reference is generally given for the generation of reluctance torque. In other words, the online full parameter estimation is always possible using the proposed algorithm if the PMSM is rotating and generating a torque, even in the steady state with no signal injection.

IV. SIMULATION VERIFICATION

The simulation to verify the effectiveness of the proposed algorithm was conducted using the PSIM software with a 15-kW IPMSM driven by a VSI, whose specifications and nominal parameters are listed in Table 1. In addition, the d- and q-axes inductances were based on functions of the d- and q-axes currents resulting from the magnetic saturation, which are expressed as follows:

$$
\begin{aligned}
L_d &= 0.5 + 0.002 i_d\,(mH),\\
L_q &= 0.95 - 0.002 i_q\,(mH).
\end{aligned} \tag{22}
$$

The switching frequency was fixed at 10 kHz, and all sensors such as the resolver, stator current, and DC-link voltage sensors had zero-mean white noises, the peak-to-peak amplitudes of which were 0.2% of the maximum output of each sensor to reflect a realistic situation. The cut-off frequency of the LPF used in the signal processing was set to $w_c = \max(w_r/6, 12.5)$, which was considered to be appropriate for satisfying the trade-off between noises/uncertainties attenuation and rapid detection of the stator current ripple amplitudes.

TABLE 1. Specifications and Nominal Parameters of the IPMSM.

Maximum torque	140 Nm
Base speed	850 rpm
Maximum stator current	200 A
DC-link voltage	144 V
Number of poles	12
Stator resistance (R_s)	142 $m\Omega$
Flux linkage (ϕ_m)	0.06 Wb

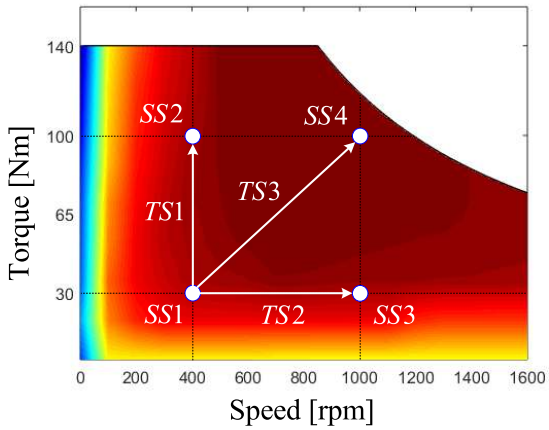

FIGURE 6. Operating conditions of the PMSM for online parameter estimation in steady states (SS1, SS2, SS3, and SS4) and transient states (TS1, TS2, and TS3).

The signal injection (SI) method introduced in [23] was adopted for a comparison. The frequency and amplitude of the injected sinusoidal current were set at 10 Hz and 5 A, which are reasonably large values, so that the injected signal was not buried in the stator current ripples. The forgetting factor of the RLS was set to 0.999 for both the proposed and signal injection methods. Both parameter estimation methods started from 0.2 s to allow time for the signal processing outputs of the proposed method to reach the target values.

The simulation was conducted for two situations: steady and transient states. The purpose of the online parameter estimation in the steady state was to determine whether the estimated values of the proposed algorithm converge to the true parameters (which are considered constant in the steady state) and examine the variations in the estimation performance based on operating conditions, in comparison with the SI method. Four operating conditions of SS1, SS2, SS3, and SS4 as shown in Fig. 6, which were all combinations of low and high levels of the output torque and rotating speed of the PMSM, were considered for the steady-state cases. The torque operating conditions were converted to the d- and

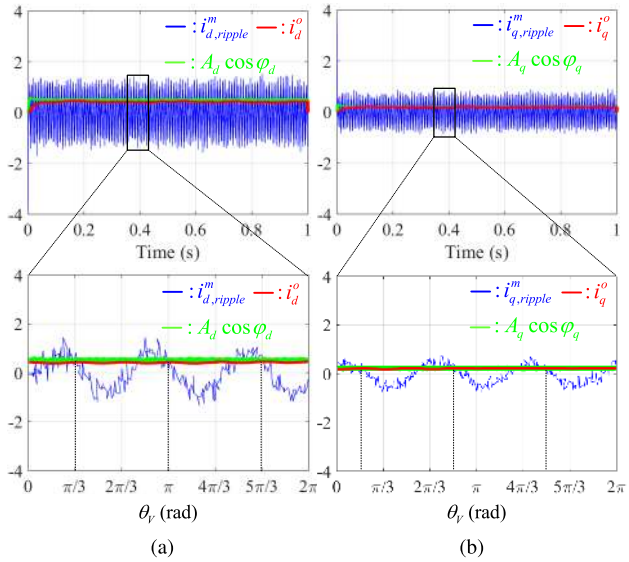

FIGURE 7. (a) *d*-axis and (b) *q*-axis current ripple measurements and outputs of signal processing under the steady-state operating conditions of SS1.

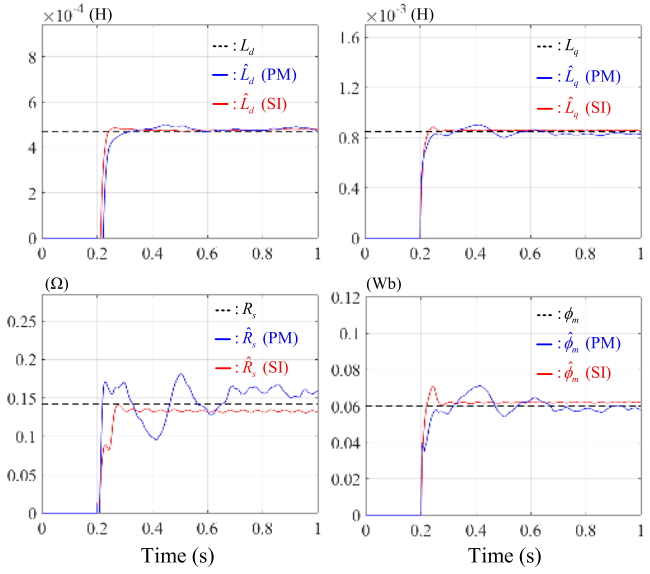

FIGURE 8. Results of online full parameter estimation under the steady-state operating conditions of SS1 (PM: proposed method, SI: signal injection method).

q-axes current references with the MTPA or FW trajectory using nominal parameters and then assigned to the PMSM current controller.

The simulation study for the transient state was conducted to examine the robustness of the proposed algorithm in the transient- and parameter-varying situations as compared to the SI method. Confirming the estimation performance for the *d*- and *q*-axes inductances is particularly important, as the inductances vary rapidly with the stator currents. Three transient cases of TS1, TS2, and TS3 as shown in Fig. 6, where the operating conditions changed from SS1 to SS2, SS3, and SS4 within one second, respectively, were considered.

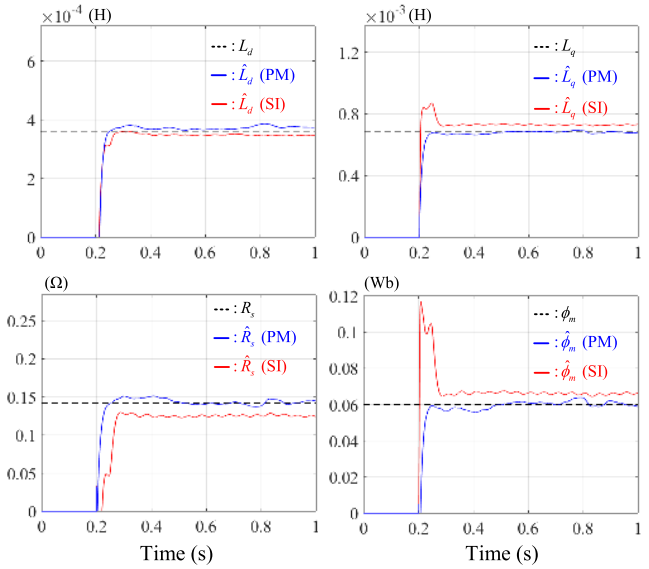

FIGURE 9. Results of online full parameter estimation under the steady-state operating conditions of SS2 (PM: proposed method, SI: signal injection method).

A. PARAMETER ESTIMATIONS IN THE STEADY STATE

Fig. 7 shows the measurements of the *d*- and *q*-axes current ripples and the outputs of their signal processing for the operating conditions of SS1. Although the current ripple measurements of $i^m_{d,ripple}$ and $i^m_{q,ripple}$ contained undesirable noises, the signal processing outputs of i^o_d and i^o_q converged to their target values of $A_d \cos\varphi_d$ and $A_q \cos\varphi_q$ within 0.1 s, suggesting that the signal processing technique can attenuate the adverse effects existing in the measurements. Because the signal processing showed similar results for the other operating conditions of SS2, SS3, and SS4, those results are not provided.

The results of online full parameter estimation under the steady-state operating conditions of SS1, SS2, SS3, and SS4 are presented in Fig. 8, 9, 10, and 11, respectively. Most estimates from both the proposed method (denoted as "PM" in the figures) and SI method approximated their true values to within 0.2 s. With respect to the proposed method, the *d*- and *q*-axes inductance estimates approximated the true values under all operating conditions except for the *d*-axis inductance estimate for SS4. The stator current ripple model was indeed a model for current variation. Therefore, it mainly contained inductance information, which was confirmed by the fact that the current ripple model of (16) is directly proportional to the inverse of the *d*- and *q*-axes inductances. Moreover, the terms that include the *d*- and *q*-axes inductances ($w_r L_{d(q)} i_{d(q)}$) in both the stator current ripple model and the state equations have a large ratio because they were multiplied by the electrical rotor speed and stator currents. These are the factors that increased the accuracy of the inductance estimation. It is assumed that the *d*-axis inductance estimation error for SS4 is caused by the error in the signal processing output of i^o_d to its target value, which should be improved in future studies. However, the stator

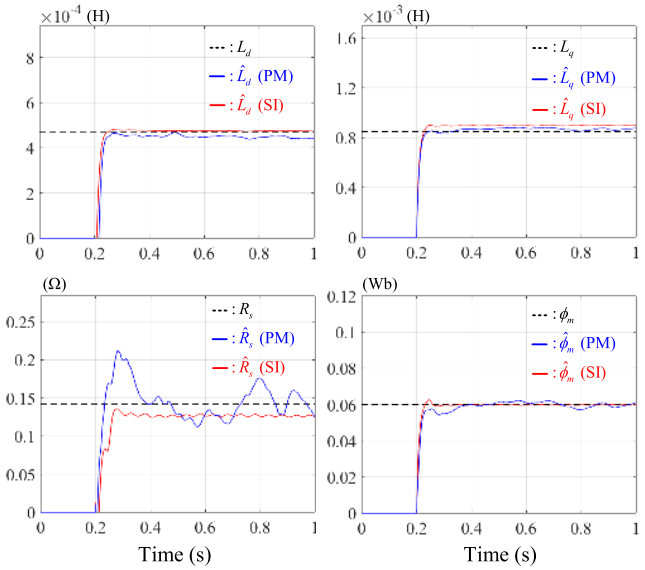

FIGURE 10. Results of online full parameter estimation under the steady-state operating conditions of SS3 (PM: proposed method, SI: signal injection method).

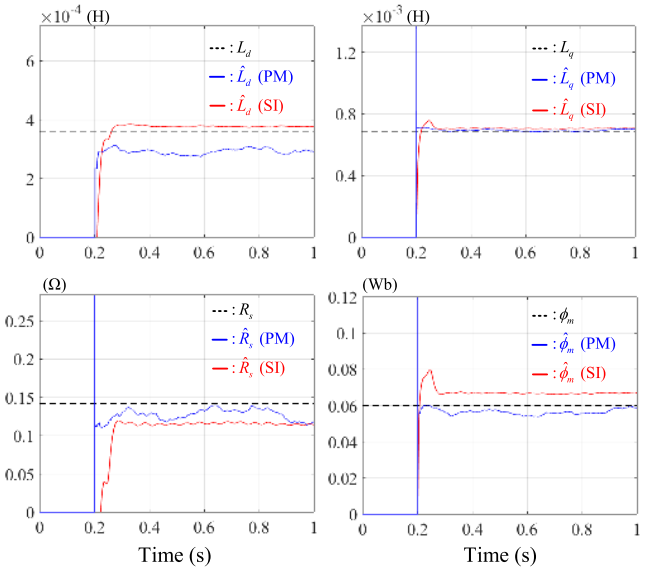

FIGURE 11. Results of online full parameter estimation under the steady-state operating conditions of SS4 (PM: proposed method, SI: signal injection method).

resistance estimates tend to fluctuate in the vicinity of the true values for SS1 and SS3. Because information about the stator resistance is obtained only by multiplying it by the stator currents, the estimates can become sensitive at low stator current conditions such as SS1 and SS3. However, because the average values of the fluctuation do not deviate greatly from the true value, the estimate can be stabilized through a tuning of the RLS forgetting factor without difficulty, which is explained in Section IV-C.

In the case of the SI method, the d- and q-axes inductance estimates nearly approximated the true values under all operating conditions because of their large ratios in the

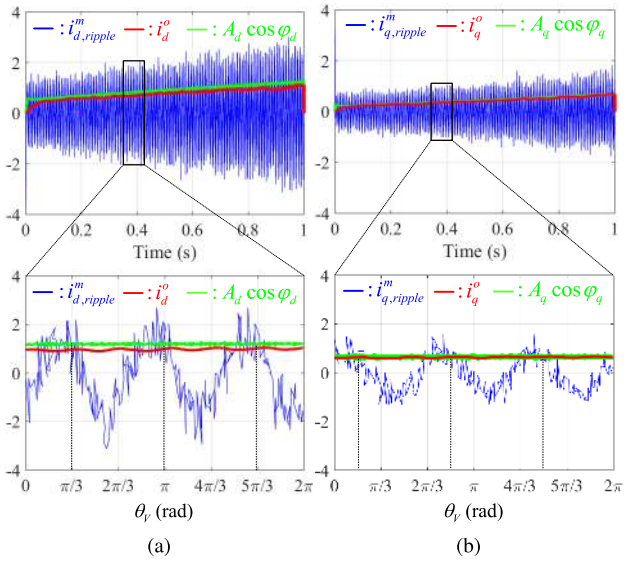

FIGURE 12. (a) d-axis and (b) q-axis current ripple measurements and outputs of signal processing for the transient-state operating conditions of TS1.

state equations. However, the flux linkage estimates deviated from the true values for SS2 and SS4. This is believed to have occurred because the injected signal becomes relatively small for high stator current conditions such as SS2 and SS4, and information obtained from the injected signal is reduced. Increasing the amplitude of the injection signal can improve the accuracy of the parameter estimation, but it can cause problems such as increases in torque ripple and copper loss as well as stability degradation, which is discussed later. The stator resistance estimates that were directly affected by the stator current tended to oscillate in the same manner as the injected signal and had a non-negligible estimation error.

Determining which of the two methods performed better in the steady state is difficult. However, that the proposed method verified its feasibility and effectiveness for the online full parameter estimation with no signal injection is meaningful.

B. PARAMETER ESTIMATIONS IN THE TRANSIENT STATE

Fig. 12 shows the measurements of the d- and q-axes current ripples and the outputs of their signal processing for the operating conditions of TS1. Although the current ripple amplitudes increased with time and contained undesirable noises, the signal processing outputs of i_d^o and i_q^o approximated the changing target values of $A_d \cos\varphi_d$ and $A_q \cos\varphi_q$ within 0.1 s, suggesting that the signal processing technique also works well in the transient state. Because the signal processing showed similar results for the other operating conditions of TS2 and TS3, those results are not provided.

The results of online full parameter estimation under the transient operating conditions of TS1, TS2, and TS3 are presented in Fig. 13, 14, and 15, respectively. In the case of the proposed method, most estimates approximated their true

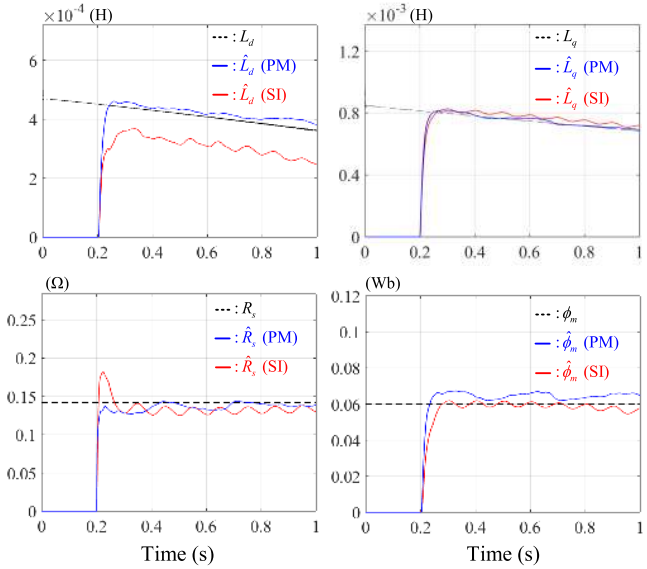

FIGURE 13. Results of online full parameter estimation under the transient operating conditions of TS1 (PM: proposed method, SI: signal injection method).

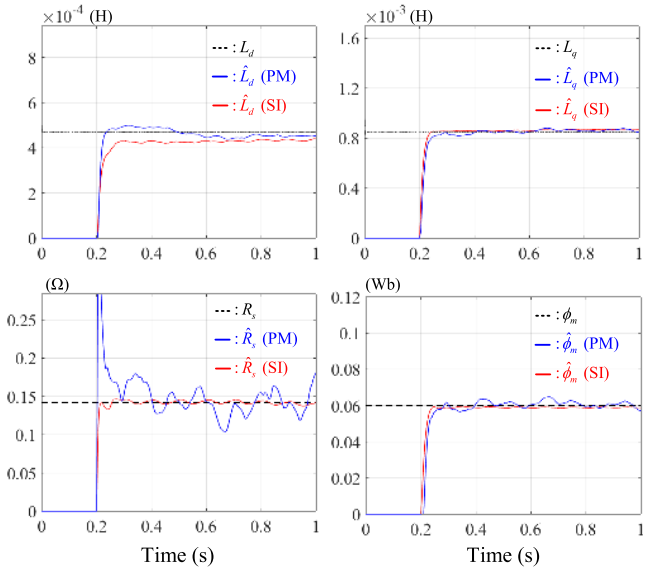

FIGURE 14. Results of online full parameter estimation under the transient operating conditions of TS2 (PM: proposed method, SI: signal injection method).

values to within 0.2 s under all operating conditions except for the d-axis inductance for TS3. In particular, the d- and q-axes inductance estimates could quickly track the true values that varied with the stator currents, which was possible with the help of the signal processing whereby the outputs rapidly converged to the target values. It is assumed that the d-axis inductance estimation error for TS3 was caused by the error in the signal processing output i_d^o to its target value, which should be improved in future studies. However, the stator resistance estimates tended to fluctuate considerably in the vicinity of the true value of TS2, where the rotor speed increased considerably. The increase in rotor speed caused

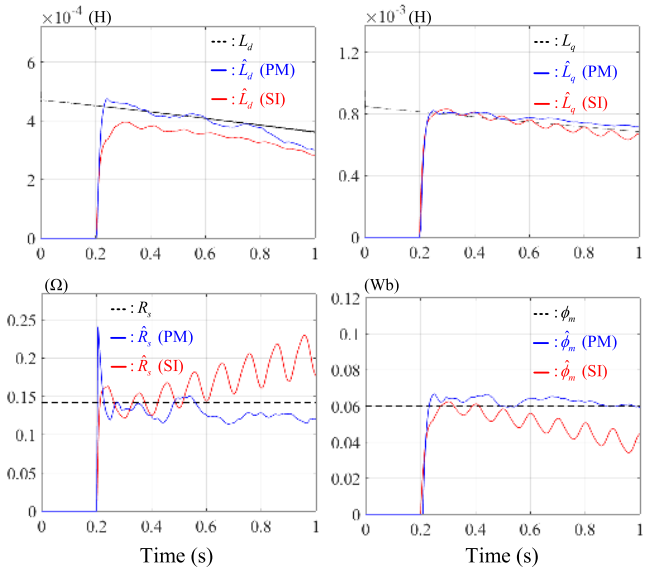

FIGURE 15. Results of online full parameter estimation under the transient operating conditions of TS3 (PM: proposed method, SI: signal injection method).

the terms containing the stator resistance to be relatively small in the parametric model, and caused the stator resistance estimates to become sensitive. However, because the average value of the fluctuation did not deviate considerably from the true value, it can be stabilized by tuning the RLS forgetting factor without difficulty, which is described in Section IV-C.

With respect to the SI method, it exhibited stable estimation performance for TS2, where only the rotor speed varied. However, for TS1 and TS3, where the stator current varied, the d-axis inductance estimates had large errors, and all estimates tended to oscillate in the same manner as the injected signal. Particularly for TS3, where both the stator current and rotor speed changed, the stator resistance and flux linkage estimates tended to oscillate considerably and deviate from their true values. This means that signal injection can act as a factor to introduce considerable disturbance and instability into the PMSM drive system under transient conditions, as mentioned in [24]. The instability is likely to become critical when the operating conditions of the PMSM are very close to the voltage or current limit, such as in SS4 or TS3. In addition, the signal injection method has an inherent an estimation error caused by parameter variations, which are themselves the result of a state change derived from the injected current into the PMSM.

C. PARAMETER ESTIMATIONS NEAR ZERO SPEED

Because six values of Θ_V are used in the stator current ripple model (16) for each electrical cycle, verifying the performance of the proposed method near zero speed, where the update rate of the model is relatively slow, is crucial. One steady-state operating condition in which the rotating speed is 40 rpm and the output torque is 30 Nm, named SS0, and one transient operating condition where the rotating speed is fixed

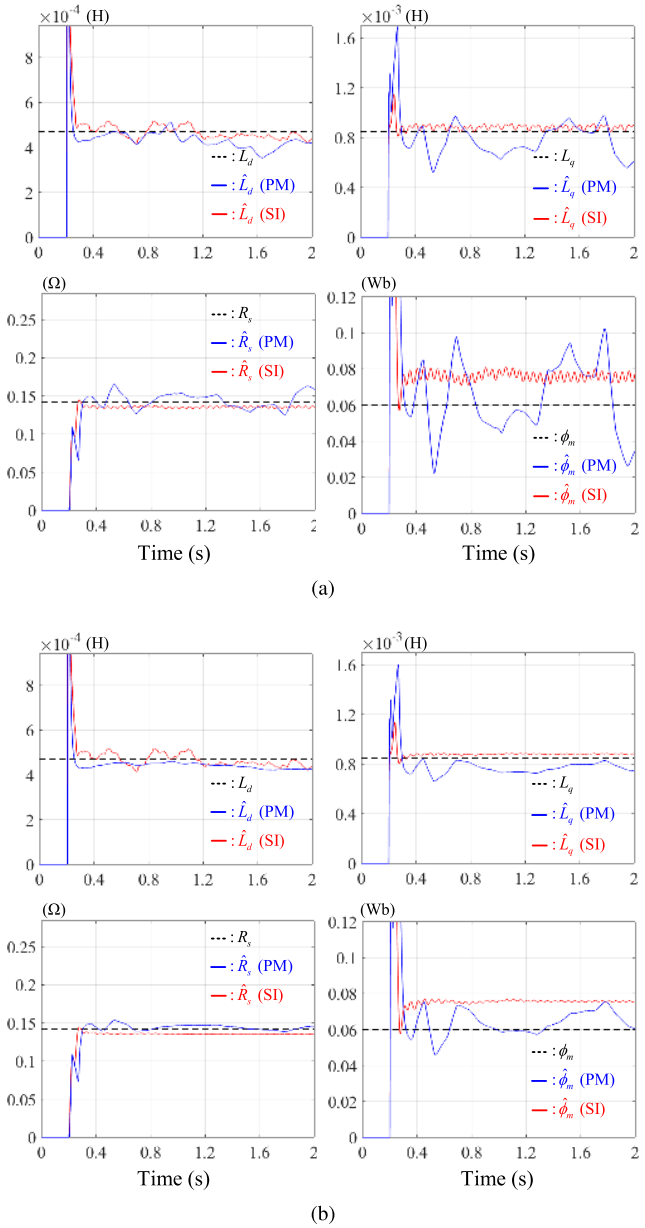

FIGURE 16. Results of online full parameter estimation under the steady-state operating conditions of SS0 (PM: proposed method, SI: signal injection method) with different forgetting factors of (a) $\mu = 0.999$ and (b) $\mu = 0.9999$.

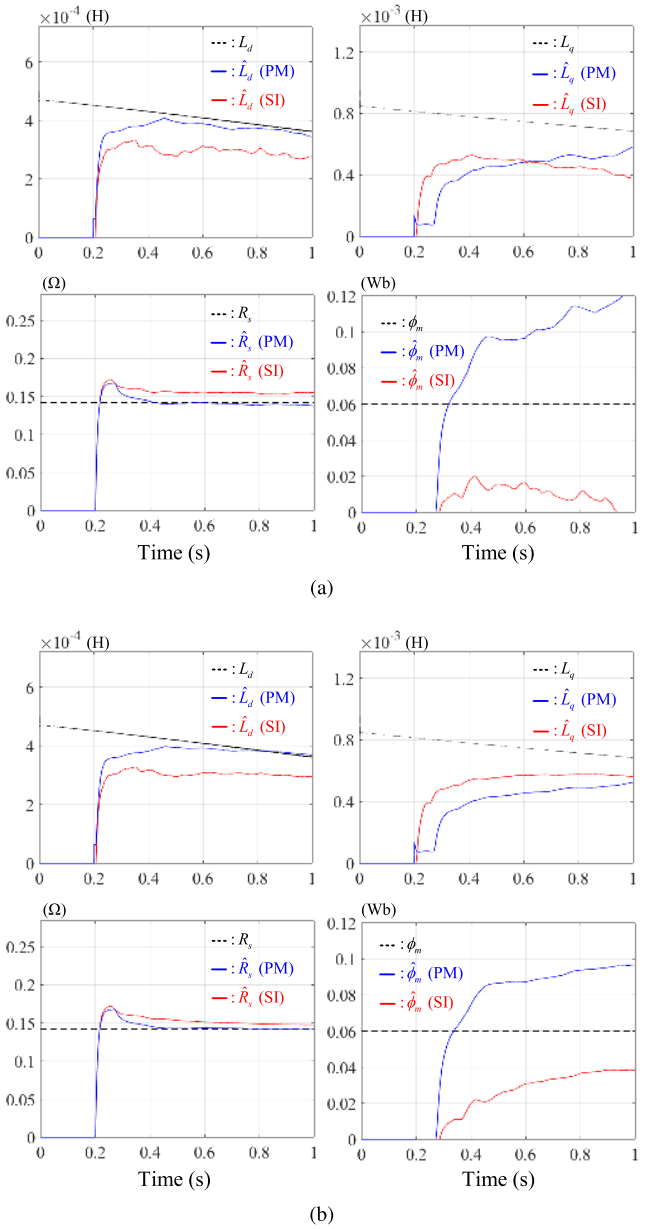

FIGURE 17. Results of online full parameter estimation under the steady-state operating conditions of TS0 (PM: proposed method, SI: signal injection method) with different forgetting factors of (a) $\mu = 0.999$ and (b) $\mu = 0.9999$.

at 40 rpm and the output torque changes from 30 to 100 Nm within 1 s, named TS0, were considered for the near zero speed cases. Two forgetting factors of $\mu = 0.999$, the same value as used in the previous simulation, and $\mu = 0.9999$ were used for both the proposed and SI methods.

The results of online full parameter estimation for SS0 are presented in Fig. 16. In the case of the proposed method with $\mu = 0.999$ (Fig. 16a), all estimates tended to fluctuate considerably in the vicinity of the true values. This was in contrast to the other steady-state cases in which at most one estimate fluctuated. The slow update rate of the stator current ripple model in low-speed operations was the main cause of the fluctuations, as the estimates were made sensitive to each update of the model. The fluctuations could be stabilized by increasing the forgetting factor to $\mu = 0.9999$, as shown in Fig. 16b. In the case of the SI method, most estimates were stabilized near to their true values regardless of the forgetting factor by utilizing rapidly updated information through high-frequency signal injection.

The results of online full parameter estimation for TS1 are presented in Fig. 17. The estimates of the d-axis inductance and the stator resistance tended to be similar to those of the case of TS0 in both methods. However, the flux linkage estimates had large estimation errors regardless of the estimation method and forgetting factor that were used. It is believed that this was because of the inevitable limit that the term

that includes flux linkage ($w_r\phi_m$) in both the stator current ripple model and the state equations considerably decreased as compared to the other terms as the torque increased at a speed approximating zero.

From the aforementioned simulation results, we can conclude that the proposed method can reliably estimate all electrical parameters of the PMSM simultaneously, not only in steady states but also in most transient states. With the SI method, estimating all parameters simultaneously by the artificial excitation to derive the addition of the rank was also possible, although it had inherent problems of torque ripple or increased copper loss. However, it was confirmed that injected signal caused an instability problem in some transient operations. From this perspective, the proposed method can be regarded as a successful solution to the rank deficiency problem in online full parameter estimation by using the hidden dynamics that exist in the stator current ripples and that do not rely on signal injection, which may involve the problems previously discussed. However, the proposed method still has difficulties estimating the flux linkage near zero speed, particularly when the output torque changes. This will be a major issue to be addressed in future studies, including for the SI method as well.

The effectiveness of the proposed method and its potential for use in a variety of applications such as torque control, fault diagnosis, and sensorless control were verified.

V. CONCLUSION

This study proposed a method for the real-time full parameter estimation of a PMSM. The rank deficiency problem was successfully resolved by introducing the stator current ripple model together with the two known state equations, even in a steady state with no signal injection. A signal processing technique to remove noises and uncertainties that exist in the stator current ripple measurements was devised. The simulation results verified that the proposed method simultaneously estimates all electrical parameters of the PMSM under most steady and transient conditions ranging from 5% to 125% of rated speed and from 20% to 70% of rated torque. The effectiveness of the proposed method on the IPMSM drives proved that it can be used in various potential applications such as torque control, fault diagnosis, and sensorless control.

REFERENCES

[1] S.-Y. Jung, J. Hong, and K. Nam, "Current minimizing torque control of the IPMSM using Ferrari's method," *IEEE Trans. Power Electron.*, vol. 28, no. 12, pp. 5603–5617, Dec. 2013.

[2] J. Lee, K. Nam, S. Choi, and S. Kwon, "Loss-minimizing control of PMSM with the use of polynomial approximations," *IEEE Trans. Power Electron.*, vol. 24, no. 4, pp. 1071–1082, Apr. 2009.

[3] J. Sun, X. Luo, and X. Ma, "Realization of maximum torque per ampere control for IPMSM based on inductance segmentation," *IEEE Access*, vol. 6, pp. 66088–66094, 2018.

[4] J. Wu, J. Wang, C. Gan, Q. Sun, and W. Kong, "Efficiency optimization of PMSM drives using field-circuit coupled FEM for EV/HEV applications," *IEEE Access*, vol. 6, pp. 15192–15201, 2018.

[5] F. Briz, M. W. Degner, and R. D. Lorenz, "Analysis and design of current regulators using complex vectors," *IEEE Trans. Ind. Appl.*, vol. 36, no. 3, pp. 817–825, May/Jun. 2000.

[6] Y. Kim, H.-T. Seo, S.-K. Kim, and K.-S. Kim, "A robust current controller for uncertain permanent magnet synchronous motors with a performance recovery property for electric power steering applications," *Energies*, vol. 11, no. 5, p. 1224, 2018.

[7] B. Aubert, J. Régnier, S. Caux, and D. Alejo, "Kalman-filter-based indicator for online interturn short circuits detection in permanent-magnet synchronous generators," *IEEE Trans. Ind. Electron.*, vol. 62, no. 3, pp. 1921–1930, Mar. 2015.

[8] S.-C. Yang, G.-R. Chen, and D.-R. Jian, "On-line stator open-phase fault detection and tolerant control for permanent magnet machines using the neutral point voltage," *IEEE Access*, vol. 5, pp. 1073–1082, 2017.

[9] S. Ruoho, J. Kolehmainen, J. Ikaheimo, and A. Arkkio, "Interdependence of demagnetization, loading, and temperature rise in a permanent-magnet synchronous motor," *IEEE Trans. Magn.*, vol. 46, no. 3, pp. 949–953, Mar. 2010.

[10] K. Liu, Z. Q. Zhu, and D. A. Stone, "Parameter estimation for condition monitoring of PMSM stator winding and rotor permanent magnets," *IEEE Trans. Ind. Electron.*, vol. 60, no. 12, pp. 5902–5913, Dec. 2013.

[11] S.-C. Yang, S.-M. Yang, and J.-H. Hu, "Robust initial position estimation of permanent magnet machine with low saliency ratio," *IEEE Access*, vol. 5, pp. 2685–2695, 2017.

[12] H. Chaoui, O. Okoye, and M. Khayamy, "Current sensorless MTPA for IPMSM Drives," *IEEE-ASME Trans. Mechatronics*, vol. 22, no. 4, pp. 1585–1593, Aug. 2017.

[13] C.-C. Hwang and Y. H. Cho, "Effects of leakage flux on magnetic fields of interior permanent magnet synchronous motors," *IEEE Trans. Magn.*, vol. 37, no. 4, pp. 3021–3024, Jul. 2001.

[14] K. M. Rahman and S. Hiti, "Identification of machine parameters of a synchronous motor," *IEEE Trans. Ind. Appl.*, vol. 41, no. 2, pp. 557–565, Mar. 2005.

[15] S. Kallio, J. Karttunen, P. Peltoniemi, P. Silventoinen, and O. Pyrhonen, "Online Estimation of Double-Star IPM Machine Parameters Using RLS Algorithm," *IEEE Trans. Ind. Electron.*, vol. 61, no. 9, pp. 4519–4530, Sep. 2014.

[16] O. C. Kivanc and S. B. Ozturk, "Sensorless PMSM drive based on stator feedforward voltage estimation improved with MRAS multiparameter estimation," *IEEE/ASME Trans. Mechatronics*, vol. 23, no. 3, pp. 1326–1337, Jun. 2018.

[17] A. Piippo, M. Hinkkanen, and J. Luomi, "Adaptation of motor parameters in sensorless PMSM drives," *IEEE Trans. Ind. Appl.*, vol. 45, no. 1, pp. 203–212, Jan. 2009.

[18] Y.-S. Han, J.-S. Choi, and Y.-S. Kim, "Sensorless PMSM drive with a sliding mode control based adaptive speed and stator resistance estimator," *IEEE Trans. Magn.*, vol. 36, no. 5, pp. 3588–3591, Sep. 2000.

[19] Y. C. Shi, K. Sun, L. P. Huang, and Y. D. Li, "Online identification of permanent magnet flux based on extended kalman filter for IPMSM drive with position sensorless control," *IEEE Trans. Ind. Electron.*, vol. 59, no. 11, pp. 4169–4178, 2012.

[20] S. Nalakath, M. Preindl, and A. Emadi, "Online multi-parameter estimation of interior permanent magnet motor drives with finite control set model predictive control," *IET Electric Power Appl.*, vol. 11, no. 5, pp. 944–951, May 2017.

[21] K. Liu, Q. Zhang, J. Chen, Z. Zhu, and J. Zhang, "Online multiparameter estimation of nonsalient-pole pm synchronous machines with temperature variation tracking," *IEEE Trans. Ind. Electron.*, vol. 58, no. 5, pp. 1776–1788, May 2011.

[22] S. J. Underwood and I. Husain, "Online parameter estimation and adaptive control of permanent-magnet synchronous machines," *IEEE Trans. Ind. Electron.*, vol. 57, no. 7, pp. 2435–2443, Jul. 2010.

[23] Q. Liu and K. Hameyer, "A fast online full parameter estimation of a PMSM with sinusoidal signal injection," in *Proc. IEEE Energy Convers. Congr. Expo. (ECCE)*, Sep. 2015, pp. 4091–4096.

[24] K. Liu and Z. Q. Zhu, "Position offset-based parameter estimation for permanent magnet synchronous machines under variable speed control," *IEEE Trans. Power Electron.*, vol. 30, no. 6, pp. 3438–3446, Jun. 2015.

[25] D. Q. Dang, M. S. Rafaq, H. H. Choi, and J.-W. Jung, "Online parameter estimation technique for adaptive control applications of interior pm synchronous motor drives," *IEEE Trans. Ind. Electron.*, vol. 63, no. 3, pp. 1438–1449, Mar. 2016.

[26] P. Pillay and R. Krishnan, "Modeling of permanent magnet motor drives," *IEEE Trans. Ind. Electron.*, vol. IE-35, no. 4, pp. 537–541, Nov. 1988.

[27] B. Stumberger, G. Stumberger, D. Dolinar, A. Hamler, and M. Trlep, "Evaluation of saturation and cross-magnetization effects in interior permanent-magnet synchronous motor," *IEEE Trans. Ind. Appl.*, vol. 39, no. 5, pp. 1264–1271, Sep. 2003.
[28] J. Guo, J. Ye, and A. Emadi, "Dc-link current and voltage ripple analysis considering antiparallel diode reverse recovery in voltage source inverters," *IEEE Trans. Power Electron.*, vol. 33, no. 6, pp. 5171–5180, Jun. 2018.
[29] H.-W. Kim, M.-J. Youn, K.-Y. Cho, and H.-S. Kim, "Nonlinearity estimation and compensation of PWM VSI for PMSM under resistance and flux linkage uncertainty," *IEEE Trans. Control Syst. Technol.*, vol. 14, no. 4, pp. 589–601, Jul. 2006.

KYUNGHWAN CHOI received the B.S. and M.S. degrees in mechanical engineering from the Korea Advanced Institute of Science and Technology, Daejeon, South Korea, in 2014 and 2016, respectively, where he is currently pursuing the Ph.D. degree with the Department of Mechanical Engineering. His current research interests include design, analysis, and control of power electronics systems and ac motor drives for electric vehicles.

YONGHUN KIM received the B.S., M.S., and Ph.D. degrees in mechanical engineering from KAIST, Daejeon, South Korea, in 2010, 2012, and 2018, respectively, where he is currently with the Eco-friendly and Smart Vehicles Center, as a Research Assistant Professor. His research interests include modeling and control of power electronics systems, mechatronics systems, and electric vehicles.

KYUNG-SOO KIM received the B.S., M.S., and Ph.D. degrees in mechanical engineering from KAIST, Daejeon, South Korea, in 1993, 1995, and 1999, respectively. He was a Chief Researcher with LG Electronics, Inc., from 1999 to 2003, and a DVD Front-end Manager with STMicroelectronics Co. Ltd., from 2003 to 2005. In 2005, he joined the Department of Mechanical Engineering, Korea Polytechnic University, Gyeonggi, South Korea, as an Assistant Professor. Since 2007, he has been with the Department of Mechanical Engineering, KAIST, as a Professor, where he is currently the Head of the CCS Graduate School of Green Transportation. His research interests include digital system design for controlled mechatronics, actuator design, and control theories, such as robust control and sliding mode control.

SEOK-KYOON KIM received the B.S. degree in electronic and IT media engineering from the Seoul National University of Science and Technology, Seoul, South Korea, in 2004, and the Ph.D. degree in electrical engineering from Korea University, Seoul, in 2014. He was with LG Electronics, as a Senior Research Engineer, from 2015 to 2016, and joined the Department of Creative Convergence Engineering, Hanbat National University, Daejeon, South Korea, in 2017. His research interests include tracking problems of power electronic applications such as power converters and motor drives, power system stabilization problems, and the development of control theory such as passivity-based control and nonlinear adaptive control.